Inorg. Chem. **2008**, *47*, 7695−7702

Inorganic Chemistry
Article

Synthesis, Structure, and Electronic Properties of a Dimer of $Ru(bpy)_2$ Doubly Bridged by Methoxide and Pyrazolate

Hershel Jude,[†] Francisca N. Rein,[‡] Peter S. White,[§] Dana M. Dattelbaum,*[,⊥] and Reginaldo C. Rocha*[,†]

Los Alamos National Laboratory, Los Alamos, New Mexico 87545, and Department of Chemistry, University of North Carolina, Chapel Hill, North Carolina 27599

Received April 22, 2008

The heterobridged dinuclear complex *cis,cis*-$[(bpy)_2Ru(\mu\text{-}OCH_3)(\mu\text{-}pyz)Ru(bpy)_2]^{2+}$ (**1**; bpy = 2,2′-bipyridine; pyz = pyrazolate) was synthesized and isolated as a hexafluorophosphate salt. Its molecular structure was fully characterized by X-ray crystallography, ^{1}H NMR spectroscopy, and ESI mass spectrometry. The compound $\mathbf{1}\cdot(PF_6)_2$ ($C_{44}H_{38}F_{12}N_{10}OP_2Ru_2$) crystallizes in the monoclinic space group $P2_1/c$ with $a = 13.3312(4)$ Å, $b = 22.5379(6)$ Å, $c = 17.2818(4)$ Å, $\beta = 99.497(2)°$, $V = 5121.3(2)$ Å^3, and $Z = 4$. The *meso* diastereoisomeric form was exclusively found in the crystal structure, although the NMR spectra clearly demonstrated the presence of two stereoisomers in solution (rac and meso forms at approximately 1:1 ratio). The electronic properties of the complex in acetonitrile were investigated by cyclic voltammetry and UV−vis and NIR−IR spectroelectrochemistries. The stepwise oxidation of the Ru^{II}−Ru^{II} complex into the mixed-valent Ru^{II}−Ru^{III} and fully oxidized Ru^{III}−Ru^{III} states is fully reversible on the time scale of the in situ (spectro)electrochemical measurements. The mixed-valent species displays strong electronic coupling, as evidenced by the large splitting between the redox potentials for the Ru(III)/Ru(II) couples ($\Delta E_{1/2} = 0.62$ V; $K_c = 3 \times 10^{10}$) and the appearance of an intervalence transfer (IT) band at 1490 nm that is intense, narrow, and independent of solvent. Whereas this salient band in the NIR region originates primarily from highest-energy of the three IT transitions predicted for Ru(II)−Ru(III) systems, a weaker absorption band corresponding to the lowest-energy IT transition was clearly evidenced in the IR region (≈3200 cm^{-1}). The observation of totally coalesced vibrational peaks in the 1400−1650 cm^{-1} range for a set of five bpy spectator vibrations in Ru^{II}−Ru^{III} relative to Ru^{II}−Ru^{II} and Ru^{III}−Ru^{III} provided evidence for rapid electron transfer and valence averaging on the picosecond time scale. Other than a relatively short Ru···Ru distance (3.72 Å for the crystalline Ru^{II}−Ru^{II} complex), the extensive communication between metal centers is attributed mostly to the π-donor ability of the bridging ligands (pyz, OMe) combined with the π-acceptor ability of the peripheral (bpy) ligands.

Introduction

Polynuclear organometallic compounds exhibiting pyrazolyl bridging ligands have been extensively studied and are widely known for a number of transition metals,[1] including ruthenium.[2] However, although dimeric complexes of polypyridine-Ru(II) bridged by an enormous variety of N-heterocyclic ligands derived from azines and azoles have been explored due to a great deal of interest in their rich redox (photo)chemistry and photophysical properties,[3] examples of such complexes containing a pyrazolyl bridging group are rare.[4−7] In fact, the unsubstituted pyrazolate anion (pyz) appeared as a ditopic (*N,N′*) bridge in only one case

* To whom correspondence should be addressed. E-mail: danadat@lanl.gov (D.M.D.), rcrocha@lanl.gov (R.C.R.).
† Materials Physics and Applications Division, Center for Integrated Nanotechnologies (MPA-CINT), Los Alamos National Laboratory.
‡ Chemistry Division, Physical Chemistry and Applied Spectroscopy (C-PCS), Los Alamos National Laboratory.
§ University of North Carolina.
⊥ Dynamic and Energetic Materials Division, Shock and Detonation Physics (DE-9), Los Alamos National Laboratory.

(1) (a) Trofimenko, S. *Prog. Inorg. Chem.* **1986**, *34*, 115. (b) Trofimenko, S. *Chem. Rev.* **1993**, *93*, 943. (c) La Monica, G.; Ardizzoia, G. A. *Prog. Inorg. Chem.* **1997**, *46*, 151. (d) Mukherjee, R. *Coord. Chem. Rev.* **2000**, *203*, 151. (e) Sadimenko, A. P. *Adv. Heterocycl. Chem.* **2001**, *80*, 157.
(2) (a) Cabeza, J. A.; Landazuri, C.; Oro, L. A.; Tiripicchio, A.; Tiripicchio-Camellini, M. *J. Organomet. Chem.* **1987**, *322*, C16. (b) Carmona, D.; Mendoza, A.; Ferrer, J.; Lahoz, F. J.; Oro, L. A. *J. Organomet. Chem.* **1992**, *431*, 87. (c) Mallick, T. K.; Das, P. K.; Roy, B. K.; Ghosh, B. K. *J. Chem. Research (S)* **1993**, 374.

10.1021/ic800719u CCC: $40.75
Published on Web 07/25/2008

of doubly bridged bis-pyrazolate complex, $[(bpy)_2Ru(\mu\text{-}pyz)_2Ru(bpy)_2](PF_6)_2$ (**2**),[4] and no singly pyz-bridged dimer of $\{Ru(bpy)_2\}$ is known to date. Likewise, despite the vast literature on oxo-, hydroxo-, or alkoxo-bridged metal systems and related chemistry, the only examples of alkoxide-bridged dimers of Ru(II)-polypyridyl complexes are $[(bpy)_2Ru(\mu\text{-}OMe)_2Ru(bpy)_2](PF_6)_2$ (**3**) and $[(bpy)_2Ru(\mu\text{-}OEt)_2Ru(bpy)_2](PF_6)_2$ (**4**).[8] A few alkoxo-bridged Ru(III) or Ru(IV) complexes of the type $[L_2Ru(\mu\text{-}OR)_2RuL_2]$ (where L = anionic O,O-ligands such as acetylacetonate or catecholate)[9] have also appeared recently as interesting cases of "all oxygen" systems with the $\{O_4Ru(\mu\text{-}O_2)RuO_4\}$ coordination core.

Both azolates and alkoxides are π-excessive in electronic nature and therefore provide an interesting class of bridging ligands (L_b) for the construction of polynuclear Ru-polypyridyl systems. Their strongly σ,π-donor ability combined with the π-acceptor character of the peripheral polypyridyl ligands (L_p) promote effective $L_p(\pi^*)$-$M(d\pi)$-$L_b(\pi)$-$M(d\pi)$-$L_p(\pi^*)$ orbital interactions and extensive electronic delocalization, as opposed to the typically weaker $L_b(\pi^*)$-mediated communication between metals in analogous systems bridged by π-deficient azines. Other than geometric factors (e.g., metal−metal distance), this difference in electronic behavior is attributed mostly to the lesser extent of energy matching between the $d\pi$ orbitals of the metal and the π^* orbitals of the electron-poor azines relative to that involving the π orbitals of the electron-rich azolates.[10] In fact, electrochemical and UV−vis−NIR spectroscopic studies provided evidence for significant coupling in both **2** and **3**,[4,8] although the electronic delocalization is much more pronounced in the latter.

Here we report the preparation and structural and electronic characterization of the μ-OMe/μ-pyz doubly bridged complex **1**, a "hybrid" of **2** and **3** as the first example of an alkoxide/azolate heterobridged dimer of the $\{Ru(bpy)_2\}$ moiety. The observed properties of **1** are interesting and indicate exceptionally strong ligand-mediated electronic coupling that is not an averaged combination of those reported for **2** and **3**.

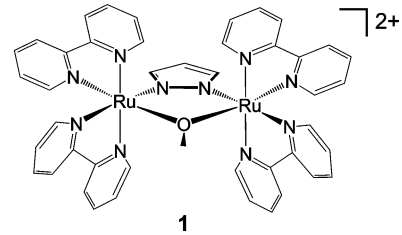

1

Experimental Section

Materials. $Ru(bpy)_2Cl_2$ was prepared as previously described.[11] Pyrazole (pyzH, Acros), sodium hydroxide (Fisher), and potassium hexafluorophosphate (Acros) were used as received. All organic solvents were high-purity grade and used without further purification. Solvents used in the preparation of solutions for electrochemical or spectroscopic experiments were anhydrous and stored over 4-Å molecular sieves. Tetrabutylammonium hexafluorophosphate (TBAH; Aldrich) was dried in vacuum prior to its use as supporting electrolyte in solutions for electrochemical experiments.

Synthesis of $[(bpy)_2Ru(\mu\text{-}OMe)(\mu\text{-}pyz)Ru(bpy)_2](PF_6)_2$ (1·$(PF_6)_2$). To 120 mL of methanol were added $Ru(bpy)_2Cl_2\cdot 2H_2O$ (1.04 g; 2.0 mmol), pyzH (67 mg; 1.0 mmol), and NaOH (160 mg; 4.0 mmol). The mixture was stirred at reflux under an Ar atmosphere for 20 h and cooled to room temperature. The resulting solution was filtered and 2 mL of a saturated solution of KPF_6 in water was added. Diethyl ether (300 mL) was added and the resulting purple precipitate was collected by vacuum filtration. The product was washed with diethyl ether (3 × 25 mL) and dried under vacuum for 30 min. (Yield: 0.41 g; 69%). Further purification was performed by column chromatography, using neutral alumina (activity I; 70−300 mesh) as the support and a toluene/acetonitrile (3:1) mixture as the eluant. The collected product was precipitated from acetonitrile with anhydrous ethyl ether and dried under vacuum. Prior to analyses, samples were recrystallized by vapor diffusion of diethyl ether into an acetone solution of **1**·$(PF_6)_2$. Yield: 55−60%. ESI-MS (*m*/*z*, positive ion mode): 1071.34. Anal. Calcd for $C_{44}H_{38}N_{10}OF_{12}P_2Ru_2\cdot 2CH_3COCH_3$: C, 45.12; H, 3.79; N, 10.52. Found: C, 45.38; H, 3.37; N, 10.89. Crystals for X-ray structural determination were grown from acetonitrile solutions.

Synthesis of $[(bpy)_2Ru(\mu\text{-}OMe)(\mu\text{-}pyz)Ru(bpy)_2](ClO_4)_2$ (1·$(ClO_4)_2$). This compound was prepared as above, except that KPF_6 was replaced with $NaClO_4$ and recrystallization of the product was not performed prior to elemental analyses. Yield: 65%. Anal. Calcd for $C_{44}H_{38}N_{10}O_9Cl_2Ru_2$: C, 47.02; H, 3.41; N, 12.46. Found: C, 46.76; H, 3.61; N, 12.34.

$[(bpy)_2Ru(\mu\text{-}OMe)(\mu\text{-}pyz)Ru(bpy)_2]^n$ (n = 3+ and 4+). The mixed-valent $Ru^{II}-Ru^{III}$ (n = 3+) and fully oxidized $Ru^{III}-Ru^{III}$ (n = 4+) species were generated in situ by controlled-potential oxidation of the starting $Ru^{II}-Ru^{II}$ (n = 2+) complex at suitable potentials (0.4 and 1.0 V vs Ag/Ag^+, respectively) in acetonitrile solutions containing 0.1 M TBAH. The electrode reactions were assumed to reach completeness after the current was less than 1% of the initial value, and no further change was observed in the spectra.

Characterization Methods. ^1H NMR spectra were collected at 298 K using a Bruker DRX-500 instrument. Spectral signals from solvents (CD_2Cl_2, CD_3CN, or CD_3COCD_3) were used as internal

(3) (a) Juris, A.; Balzani, V.; Barigelletti, F.; Belser, P.; von Zelewsky, A. *Coord. Chem. Rev.* **1988**, *84*, 85. (b) Sauvage, J.-P.; Collin, J.-P.; Chambron, J.-C.; Guillerez, S.; Coudret, C.; Balzani, V.; Barigelletti, F.; De Cola, L.; Flamigni, L. *Chem. Rev.* **1994**, *94*, 993. (c) Balzani, V.; Juris, A.; Venturi, M.; Campagna, S.; Serroni, S. *Chem. Rev.* **1996**, *96*, 759. (d) McCleverty, J. A.; Meyer, T. J., Eds.; *Comprehensive Coordination Chemistry II*; Elsevier: 2004; Vol. *1, 5.* (e) Vos, J. G.; Kelly, J. M. *Dalton Trans.* **2006**, 4869. (f) Constable, E. C. *Chem. Soc. Rev.* **2007**, *36*, 246.

(4) Sullivan, B. P.; Salmon, D. J.; Meyer, T. J.; Peedin, J. *Inorg. Chem.* **1979**, *18*, 3369.

(5) (a) Baitalik, S.; Florke, U.; Nag, K. *Inorg. Chem.* **1999**, *38*, 3296. (b) Baitalik, S.; Florke, U.; Nag, K. *J. Chem. Soc., Dalton Trans.* **1999**, 719. (c) Baitalik, S.; Florke, U.; Nag, K. *Inorg. Chim. Acta* **2002**, *337*, 439.

(6) Catalano, V. J.; Craig, T. J. *Inorg. Chem.* **2003**, *42*, 321.

(7) Sens, C.; Romero, I.; Rodriguez, M.; Llobet, A.; Parella, T.; Benet-Buchholz, J. *J. Am. Chem. Soc.* **2004**, *126*, 7798.

(8) (a) Bardwell, D. A.; Jeffery, J. C.; Joulié, L. F.; Ward, M. D. *J. Chem. Soc., Dalton Trans.* **1993**, 2255. (b) Bardwell, D. A.; Horsburgh, L.; Jeffery, J. C.; Joulié, L. F.; Ward, M. D.; Webster, I.; Yellowees, L. J. *J. Chem. Soc., Dalton Trans.* **1996**, 2527.

(9) (a) Miyasaka, H.; Chang, H.-C.; Mochizuki, K.; Kitagawa, S. *Inorg. Chem.* **2001**, *40*, 3544. (b) Kar, S.; Chanda, N.; Mobin, S. M.; Datta, A.; Urbanos, F. A.; Puranik, V. G.; Jimenez-Aparicio, R.; Lahiri, G. K. *Inorg. Chem.* **2004**, *43*, 4911. (c) Hashimoto, T.; Kawamoto, Y.; Ishitobi, Y.; Sasaki, T.; Fukuda, Y.; Yamagishi, A.; Sato, H.; Shimizu, K.; Hayashita, T. *Chem. Lett.* **2007**, *36*, 1174.

(10) Browne, W. R.; Hage, R.; Vos, J. G. *Coord. Chem. Rev.* **2006**, *250*, 1653.

(11) Sullivan, B. P.; Salmon, D. J.; Meyer, T. J. *Inorg. Chem.* **1978**, *17*, 3334.

Table 1. Summary of X-ray Crystallographic Data, Intensity Collection, and Structure Refinement Parameters for $\mathbf{1}\cdot(PF_6)_2$

empirical formula	$C_{44}H_{38}F_{12}N_{10}OP_2Ru_2$
fw, g/mol	1214.92
space group	$P2_1/c$
a, Å	13.3312(4)
b, Å	22.5379(6)
c, Å	17.2818(4)
α, deg	90
β, deg	99.497(2)
γ, deg	90
V, Å^3	5121.3(2)
ρ_{calcd}, g cm^{-3}	1.557
Z	4
λ(Mo Kα), Å	0.71073
T, K	100(2)
GOF	1.103
R_1 [$I > 2\sigma(I)$]	0.0419
wR_2 [$I > 2\sigma(I)$]	0.1006
R_1 (all data)	0.0526
wR_2 (all data)	0.1055

Table 2. Selected Bond Distances (Å) and Angles (deg) for $\mathbf{1}\cdot(PF_6)_2$

distances (Å)		angles (deg)	
Ru1−O2	2.139(3)	N3−Ru1−N8	92.19(14)
Ru1−N3	2.076(3)	N3−Ru1−N19	169.67(15)
Ru1−N8	2.063(4)	N3−Ru1−N20	88.17(12)
Ru1−N19	2.057(4)	N3−Ru1−N31	92.33(13)
Ru1−N20	2.032(3)	N3−Ru1−O2	84.51(11)
Ru1−N31	2.043(4)	N8−Ru1−N19	77.79(17)
N3−N7	1.372(4)	N8−Ru1−N20	94.45(13)
Ru2−O2	2.144(2)	N8−Ru1−N31	171.63(14)
Ru2−N7	2.074(3)	N8−Ru1−O2	94.67(12)
Ru2−N32	2.044(3)	N19−Ru1−N20	95.04(13)
Ru2−N43	2.027(3)	N19−Ru1−N31	97.93(16)
Ru2−N44	2.041(3)	N19−Ru1−O2	93.71(12)
Ru2−N55	2.052(3)	N20−Ru1−N31	78.66(13)
Ru1···Ru2	3.715	N20−Ru1−O2	168.51(11)
		N31−Ru1−O2	92.78(13)
		Ru1−N3−N7	123.9(2)
		Ru2−N7−N3	124.1(2)
		Ru1−O2−Ru2	120.33(11)

resonances. Electrospray ionization (ESI) mass spectrometry was performed using an Applied Biosystems QStar XL instrument equipped with a Protana Nanospray source. Samples were introduced into a coated spray needle and mounted onto the nanospray source. Elemental microanalyses were carried out by Atlantic Microlab (Norcross, GA). UV−vis absorption spectra were recorded on a Cary 300 spectrophotometer. A Bioanalytical Systems CV-50W potentiostat was used in electrochemical experiments. In cyclic voltammetry, a standard three-electrode setup consisted of a Pt disk (1.6 mm) working electrode, a Pt wire auxiliary electrode, and a Ag wire immersed in a CH_3CN solution containing 0.01 M $AgNO_3$ and 0.10 M $TBAPF_6$ as the Ag/Ag^+ reference electrode.[12] Near-IR and IR spectroscopic measurements of solution samples were performed with a Bruker Equinox 55 Fourier transform instrument. Spectra were collected in a dry nitrogen atmosphere at 1 cm^{-1} resolution (spectra were averages of 32 scans). NIR−IR spectroelectrochemical measurements were carried out using an optically transparent thin-layer electrochemical (OTTLE) cell with an internal optical path length of 100 μm between CaF_2 cell windows and a three-electrode system with a Au minigrid as working electrode; in the UV−vis spectroelectrochemistry, a quartz cell (1.0 mm) and a Pt screen were used. All electrochemical and spectroscopic experiments were conducted at room temperature.

X-ray Crystallography. Diffraction data for single crystals of $\mathbf{1}\cdot(PF_6)_2$ were collected for $2\theta < 50°$ on a Bruker-AXS SMART Apex-II diffractometer. The structure was solved by direct methods and hydrogen atoms were included in the final refinement cycles at predicted positions. The final structure contained disordered solvent that could not be modeled conventionally. The Platon Squeeze function was used, resulting in a solvent volume of 170 Å^3 containing about 36 electrons.

The crystal and refinement parameters are listed in Table 1, and selected bond lengths and angles for $\mathbf{1}\cdot(PF_6)_2$ are listed in Table 2. Additional details and complete tables of bond lengths and angles are given in Supporting Information.

(12) This Ag/Ag^+ reference electrode gave a half-wave potential ($E_{1/2}$) of 0.10 V for the ferrocene/ferrocenium couple.

Results and Discussion

Synthesis and Structural Characterization. The preparation of **1** arose from initial attempts to synthesize the singly bridged complex $[(bpy)_2(Cl)Ru(\mu\text{-pyz})Ru(Cl)(bpy)_2]^+$. By refluxing stoichiometric amounts of *cis*-$Ru(bpy)_2Cl_2$ and pyrazole (2:1) in methanol, in the presence of excess sodium hydroxide, the doubly heterobridged (μ-OMe, μ-pyz) complex **1** was formed in good yields (~70%). The dark purple product is very soluble in polar solvents such as acetonitrile, dichloromethane, and dimethylformamide. Attempts to synthesize analogues with 3,5-substituted pyrazoles (e.g., dimethylpyrazole) using similar procedures were unsuccessful and resulted in the formation of the bis-methoxide bridged dimer **3**, which was previously reported by Ward and colleagues.[8] Also unsuccessful were the attempts to prepare $[(bpy)_2Ru(\mu\text{-OEt})(\mu\text{-pyz})Ru(bpy)_2](PF_6)_2$ by (i) replacing methanol with ethanol in the above procedure and (ii) by exchanging the methoxide bridge with ethoxide (NaOEt) in dry ethanol.[8]

The ESI mass spectrum (Figure 1) displays a single major charge state at $m/z = 1071.34$, which is consistent with the formulation of the dicationic complex **1** plus one PF_6^- counterion, that is, $\{\mathbf{1}\cdot PF_6\}^+$. The isotopic patterns for all peaks are in good agreement with the predicted isotopic distribution patterns.

Dimeric complexes derived from the *cis*-$Ru(bpy)_2$ moiety exist in two diastereoisomeric forms, *racemic* (*rac*) and *meso*,[13] owing to the inherent chirality (Λ/Δ)[14] on each of the metal centers that, overall, gives three possible enantiomeric pair configurations ($\Delta\Delta/\Lambda\Lambda$ (rac) and $\Lambda\Delta \equiv \Delta\Lambda$(meso)) by which the bpy ligands on one moiety are spatially arranged above and below the bridging-ligand plane with respect to the other moiety (i.e., parallel (rac) vs orthogonal (meso)). From the ^{1}H NMR spectrum of **1** in acetone-d_6

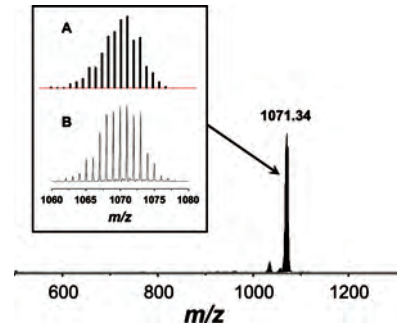

Figure 1. Electrospray ionization (ESI) quadrupole mass spectrum showing the $\{\mathbf{1}\cdot PF_6\}^+$ species. The calculated (A) and experimental (B) isotopic patterns are shown in the inset.

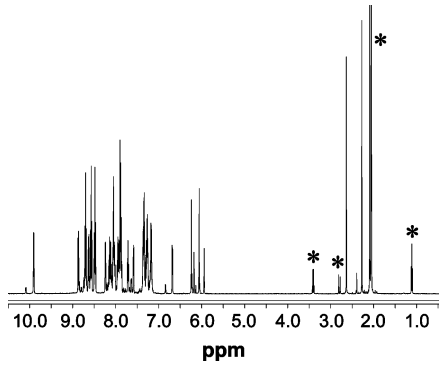

Figure 2. ^{1}H NMR spectrum of **1** in acetone-d_6. Solvent resonance peaks are marked by ∗.

(Figure 2), it is evident that two stereoisomers are present in solution. The resonances at 2.27 and 2.63 ppm (for a pair of isomers) arise from the methyl protons on the methoxide bridge and are similar to those observed for **3** (2.25 ppm; CH_3) and **4** (2.70 ppm; CH_2). The spectrum also exhibits two sets of resonances at 6.24(*d*)/6.14(*t*) and at 6.04(*d*)/5.94(*t*), which are assigned to the pyrazolate protons. As determined from the integration of these methoxide and pyrazolate resonances, two stereoisomers are present at an approximately 1:1 ratio. The region between 6.6 and 9.0 ppm is typically assigned to the bipyridine protons and complicated by the presence of multiple overlapping signals. If one of the methyl resonances is assigned a reference area value of three protons, the aromatic resonances integrate to the expected total of 64 protons (consistent with a pair of stereoisomers at nearly equal concentrations).

The molecular structure of **1**·$(PF_6)_2$ was confirmed by single-crystal X-ray diffraction. Crystals were grown by vapor diffusion of diethyl ether into acetonitrile solutions of the complex. Despite the presence of two stereoisomers in solution, as evidenced by ^{1}H NMR spectroscopy, only the meso form was detected in the crystal structure. This observation is somewhat surprising because the rac stereoisomer was exclusively found[8] in the related complexes **3** and **4**, for which it was concluded that the meso configuration could not be formed owing to steric effects.

ORTEP diagrams of the cation are shown in Figure 3, and relevant data are summarized in Table 2. The geometry about the Ru centers is a distorted octahedral, with angles in the 78−98° and 169−175° ranges.[15] The largest deviations from the ideal 90° and 180° angles are largely dictated by the oxygen (O2) coordinating atom of the methoxide group, for which the Ru−O−Ru angle (120.3°) and short bridging length (through-bond Ru−Ru distance: 4.28 Å) impose a constrained geometry relative to the opposite pyrazolate coligand (through-bond Ru−Ru distance: 5.52 Å). The Ru−N(bpy), Ru−N(pyz), and Ru−O(OR) distances are consistent with those typically found in Ru(II) complexes.[6—8,16] The geometric through-space Ru···Ru distance

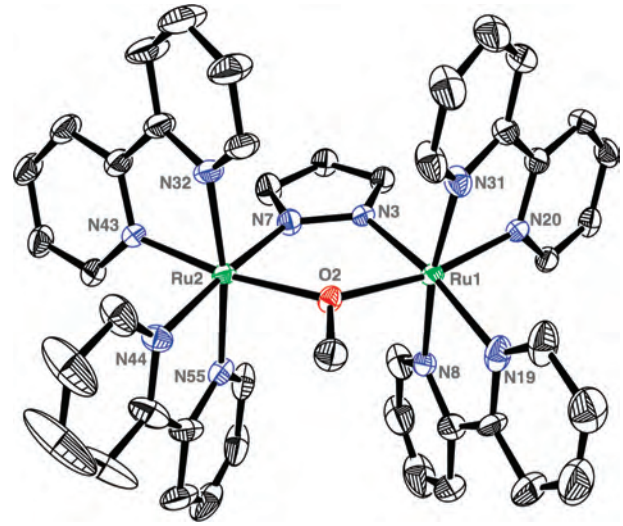

Figure 3. X-ray crystal structure of **1**·$(PF_6)_2$. H atoms and PF_6^- counterions are omitted for clarity (ORTEP plot drawn at 50% probability).

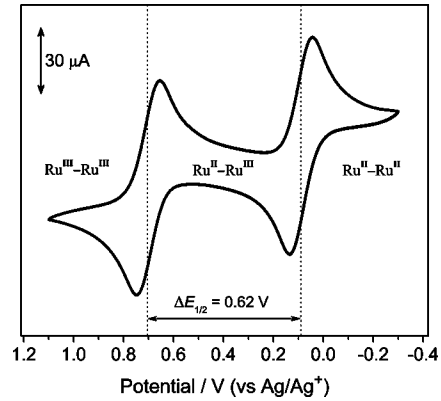

Figure 4. Cyclic voltammogram of **1** (5.0 mM) in acetonitrile (0.1 M TBAH); the 2nd and 3rd complete cycles at a scan rate of 50 mV s^{-1} are shown in the figure.

(3.72 Å) in crystalline **1**·$(PF_6)_2$ is similar to pyrazolyl-bridged ruthenium dimers with a second single-atom bridging ligand, such as [(tpy)Ru(μ-Cl)(μ-bpp)Ru(tpy)]$(PF_6)_2$ (d_{Ru-Ru} = 3.88 Å;[7] tpy = 2,2′;6′,2″-terpyridine and bpp = 3,5-bis(pyridine-2-yl)pyrazolate) and [(tpy)Ru(μ-Cl)(μ-dmbpp)Ru(tpy)]-$(PF_6)_2$ (d_{Ru-Ru} = 3.86 Å and 3.89 Å;[6] dmbpp = 3,5-bis(6-methylpyridine-2-yl)pyrazolate, and 3,5-bis(4-methylpyridine-2-yl)pyrazolate, respectively). As expected, however, the separation between the two Ru atoms is shorter in crystals of the bis-methoxide complex **3** (d_{Ru-Ru} = 3.32 Å).[8]

Electrochemistry. The cyclic voltammogram of **1** in acetonitrile (Figure 4) shows two one-electron processes at 0.09 and 0.71 V versus Ag/Ag^+.[12] These redox processes are clearly reversible and correspond to the $Ru^{II}-Ru^{II}/Ru^{II}-Ru^{III}$ and $Ru^{II}-Ru^{III}/Ru^{III}-Ru^{III}$ couples, respectively. Overlapping one-electron processes are also observed below −1.7 V and are characteristic of the closely spaced reductions of the bpy ligands. The chemical stability of the mixed-valent $Ru^{II}-Ru^{III}$ and fully oxidized $Ru^{III}-Ru^{III}$ was also verified by cyclic voltammetry following controlled-potential electrolysis at 0.40 and 1.0 V, respectively. The large separation between the redox potentials ($\Delta E_{1/2}$ = 0.62 V) gives a

(13) (a) Keene, F. R. *Coord. Chem. Rev.* **1997**, *166*, 121. (b) Keene, F. R. *Chem. Soc. Rev.* **1998**, *27*, 185.
(14) Δ and Λ designate right- and left-handed chirality, respectively.
(15) See also Supporting Information.
(16) Eggleston, D. S.; Goldsby, K. A.; Hodgson, D. J.; Meyer, T. J. *Inorg. Chem.* **1985**, *24*, 4573.

comproportionation constant (K_c)[17,18] of 3.0×10^{10}, which reflects the stabilization of the mixed-valent $Ru^{II}-Ru^{III}$ state relative to its reduced $Ru^{II}-Ru^{II}$ and oxidized $Ru^{III}-Ru^{III}$ isovalent counterparts.

$$Ru^{III}-Ru^{III}+Ru^{II}Ru^{II} \overset{K_c}{\rightleftharpoons} 2Ru^{II}-Ru^{III}$$

Such a large value of K_c also suggests that there is strong electronic communication between the redox centers. For comparison, this K_c value for **1** is 4 orders of magnitude larger than that for the bis-pyrazolate bridged complex, **2** ($\Delta E_{1/2} = 0.38$ V; $K_c = 2.7 \times 10^6$),[4] and 10 times larger than that observed for the bis-methoxide bridged complex, **3** ($\Delta E_{1/2} = 0.55$ V; $K_c = 3 \times 10^9$),[8] all at identical experimental conditions (acetonitrile; 0.1 M TBAH). However, electrochemical properties alone cannot be taken as conclusive evidence for electronic localization or delocalization between charge centers. For instance, although a large separation between the Ru(II)/Ru(III) potentials was observed in the case of the bis-chloro bridged dimer, $[(bpy)_2Ru(\mu\text{-}Cl)_2Ru(bpy)_2]^{2+}$ ($\Delta E_{1/2} = 0.55$ V), it was concluded that the redox splitting arises because of electrostatic effects and not because of extensive delocalization in the mixed-valent $Ru^{II}-Ru^{III}$ ion.[19] A similar conclusion was suggested for the bis-pyrazolyl complex, whose mixed-valent form is unstable and undergoes an asymmetrical cleavage upon oxidation from the isolated $Ru^{II}-Ru^{II}$ species.[4] A better probe for estimating the extension of electronic communication and localization vs delocalization in mixed-valence systems is the set of intervalence transfer (IT) absorption bands that usually appear in the near-infrared (NIR) region for complexes with significant ligand-mediated metal-to-metal interactions (see later).

Electronic Spectra. The UV−vis absorption spectra of **1** at all three $Ru^{II}-Ru^{II}$, $Ru^{II}-Ru^{III}$, and $Ru^{III}-Ru^{III}$ oxidation states were obtained in situ by spectroelectrochemistry in acetonitrile (Figure 5,) starting from the purple solution of the isolated hexafluorophosphate salt of the dicationic $Ru^{II}-Ru^{II}$ species. Consistent with the results of cyclic voltammetry, the spectroelectrochemical stepwise processes were all reversible, as indicated by the complete spectral recovery upon reduction/oxidation cycles.

The visible spectrum of the fully reduced $Ru^{II}-Ru^{II}$ starting complex features absorptions in the broad range from 300 to 700 nm, with two main regions around 300−450 and 450−650 nm consisting of at least two components each ($\lambda_{max} \approx 350$, 400, 490, 540, and 600_{sh} nm). These overlapping bands are characteristic of metal-to-ligand charge-transfer (MLCT) processes involving multiple, closely spaced transitions from the dπ orbitals of Ru(II) to the low-lying π^* orbitals of bpy. The lower MLCT energies of **1** compared to all-polypyridyl Ru complexes reflect the π-donating nature of the bridging ligands, which results in a decreased energy

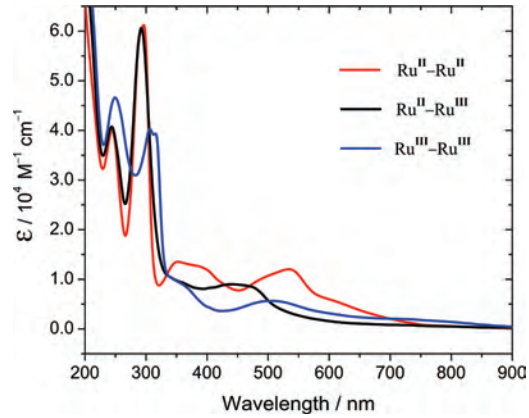

Figure 5. UV−vis spectra of **1** in acetonitrile. The $Ru^{II}-Ru^{III}$ and $Ru^{III}-Ru^{III}$ species were electrogenerated in situ by stepwise oxidation of the starting $Ru^{II}-Ru^{II}$ complex at 0.4 and 1.0 V vs Ag/Ag^+, respectively. The oxidation steps were fully reversible and the initial spectrum of $Ru^{II}-Ru^{II}$ was recovered upon reduction.

separation between the Ru(dπ) and bpy(π^*) levels. The more intense bands in the UV region (λ_{max} at 244 and 296 nm) are typical of bpy systems and originate from ligand-centered bpy(π)→bpy(π^*) transitions.[20] It is also worth noting that the MLCT energies for the isolated $Ru^{II}-Ru^{II}$ forms of **1**, **2**,[4] and **3**[8] follow the order **2**> **1**> **3**, indicating therefore that O-methoxide is a stronger $\pi(p_\pi)$ electron donor than *N*,*N*-pyrazolate. This assessment is in agreement with the relative basicities of these ligands (pK_a values are 14.2 for pyzH and 15.5 for MeOH), owing to the increased hardness (i.e., localization of charge density) of the coordinating oxygen atom at OMe compared to the nitrogen atoms of pyz.

The visible spectrum of the fully oxidized $Ru^{III}-Ru^{III}$ species, in turn, is dominated by ligand-to-metal charge-transfer (LMCT) transitions involving the high-lying π orbitals of the bridging ligands and the semioccupied dπ orbitals of the Ru(III) centers. In addition to the well-defined band with λ_{max} at 507 nm, a broad and weak absorption that extends up to ∼850 nm is shown. LMCT transitions involving the low-lying π orbitals of bpy ligands may also occur, but the resulting absorptions are presumably precluded by the highly intense UV bands from the bpy internal transitions. The shoulder at ∼350 nm (which is less evident but also appears for $Ru^{II}-Ru^{III}$) can be tentatively assigned to such a transition.

At the intermediate mixed-valent $Ru^{II}-Ru^{III}$ state (trication), the stronger visible absorption is defined between 400 and 500 nm (with $\lambda_{max} \approx 450$ nm), a region in which neither $Ru^{II}-Ru^{II}$ nor $Ru^{III}-Ru^{III}$ features absorption maxima for the corresponding MLCT/LMCT bands. The fact that the electronic spectrum for the mixed-valent $Ru^{II}-Ru^{III}$ species does not result from a half-sum of the spectra of the two isovalent $Ru^{II}-Ru^{II}$ and $Ru^{III}-Ru^{III}$ species reflects a significant perturbation of the spectroscopic redox orbitals in $Ru^{II}-Ru^{III}$ owing to strong ligand-mediated electronic interactions between metal centers. This observation is well

(17) $K_c = \exp[(RT \cdot \Delta E_{1/2})/nF] = \exp(\Delta E_{1/2}/25.69)$ for $n = 1$, $T = 298$ K, and $\Delta E_{1/2}$ in mV.
(18) Richardson, D. E.; Taube, H. *Coord. Chem. Rev.* **1984**, *60*, 107.
(19) Johnson, E. C.; Sullivan, B. P.; Salmon, D. J.; Adeyemi, S. A.; Meyer, T. J. *Inorg. Chem.* **1978**, *17*, 2211.
(20) Bryant, G. M.; Fergusson, J. E.; Powell, H. K.J. *Aust. J. Chem.* **1971**, *24*, 257.

aligned with the electrochemical findings based on the magnitude of $\Delta E_{1/2}$ and K_c values.

The most obvious spectral manifestation of mixed valency in complexes with significant ligand-mediated metal-to-metal interactions is the absorbance from intervalence transfer (IT) transitions that usually appear in the near-infrared (NIR) region as a result of the photoinduced electron transfer between the ligand-bridged redox centers with differing valences (i.e., the photoinduced interconversion of "electronic isomers": $M^n - L - M^{n+1} \xrightarrow{h\nu} M^{n+1} - L - M^n$).[21,22] NIR absorption bands are featured by delocalized (class III)[23] systems as well, but these arise from MO level transitions (analogous to bonding(π) to antibonding(π^*) transitions in organic molecules) and, due to solvent and vibrational decoupling, are much narrower than those for typically valence-localized (class II)[23] systems. A complicating issue in $d\pi^6-d\pi^5$ transition-metal systems such as Ru(II)−Ru(III) complexes is that three possible IT transitions originate from the multiple ligand-mediated electronic interactions involving the two sets of split $d\pi$ orbitals, as schematically depicted below.[24,25] Although all three transitions from the occupied orbitals ($d\pi_1^2$,$d\pi_2^2$,$d\pi_3^2$) at the donor to the hole ($d\pi_3^1$) at the acceptor contribute to define mixed-valence properties, the higher-energy IT(2,3) transitions are accompanied by the formation of interconfigurational excited states at the donor (i.e., $d\pi_1^2$,$d\pi_2^1$,$d\pi_3^2$ and $d\pi_1^1$,$d\pi_2^2$,$d\pi_3^2$) and information about genuinely *ground-state* mixed valency should thus come from analysis of the lowest-energy IT(1) band associated with the $d\pi_3^2 \rightarrow d\pi_3^1$ transition.[21,24] However, because the energy splittings between these transitions are dictated by low-symmetry and the magnitude of spin−orbit coupling, the resulting IT absorptions in Ru systems (for which $\zeta \approx 1000$ cm^{-1}) are generally closely spaced/overlapping. The relevant IT(1) band, in particular, is usually of low absorptivity and difficult to probe in the IR region.[25]

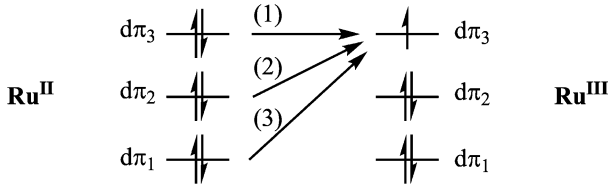

As an attempt to gain additional insight into the electronic structure of **1**, we performed and include here NIR/IR spectroscopic studies. As with the UV−vis measurements, the NIR−IR absorption spectra of **1** at all three $Ru^{II}-Ru^{II}$, $Ru^{II}-Ru^{III}$, and $Ru^{III}-Ru^{III}$ oxidation states were investigated in situ by spectroelectrochemistry in acetonitrile. While both fully reduced $Ru^{II}-Ru^{II}$ and fully oxidized $Ru^{III}-Ru^{III}$ species are transparent in the NIR region, the mixed-valent $Ru^{II}-Ru^{III}$ complex features a strong ($\varepsilon = 6.8 \times 10^3$ M^{-1} cm^{-1}) and narrow (fwhm $\approx 2.5 \times 10^3$ cm^{-1}) absorption with maximum intensity at 6.7×10^3 cm^{-1} (Figure 6). Also exclusive to the mixed-valent species is a weaker absorption band that appears in the IR region ($\tilde{\nu} \approx 3.2 \times 10^3$ cm^{-1}; with $\varepsilon \approx 6 \times 10^2$ M^{-1} cm^{-1} and $\Delta\tilde{\nu}_{1/2} \approx 1.7 \times 10^3$ cm^{-1}).[26] No significant evidence for further absorptions due to electronic transitions (such as possible interconfigurational (IC) transitions[24,25]) was found below 2000 cm^{-1}. Whereas the IR band is attributed to the lowest-energy IT(1) transition, the strong NIR absorption is most likely a convolution of both IT(2) and IT(3) bands.

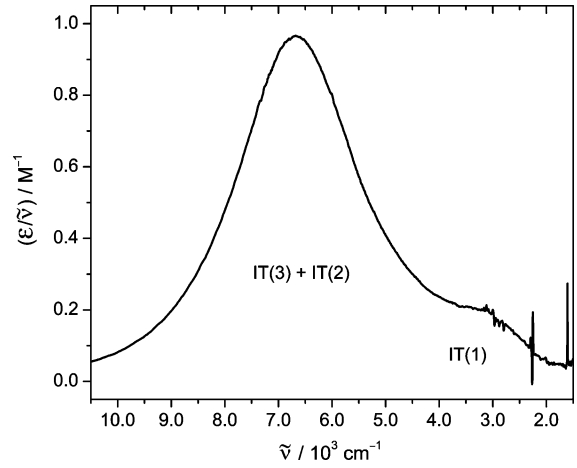

Figure 6. NIR−IR spectrum of the mixed-valent form of **1** in acetonitrile-d_3. This $Ru^{II}-Ru^{III}$ species was electrogenerated in situ by oxidation of the starting complex at 0.4 V vs Ag/Ag$^+$. The process was fully reversible and the initial spectrum of $Ru^{II}-Ru^{II}$ was recovered upon reduction. The initial spectrum (ε vs $\tilde{\nu}$) was rescaled as $\varepsilon/\tilde{\nu}$ vs $\tilde{\nu}$.[27,28]

A useful diagnostic test for localized vs delocalized behavior is based on the comparison of the experimental IT bandwidth (fwhm or $\Delta\tilde{\nu}_{1/2}^{exp}$) with the theoretical values ($\Delta\tilde{\nu}_{1/2}^{calcd} = (2310\tilde{\nu}_{max})^{1/2}$ at 298 K).[27] Because charge localization at the weak coupling limit is assumed in the classical two-state model for the calculation of $\Delta\tilde{\nu}_{1/2}^{calcd}$, a substantial deviation due to narrow experimental widths relative to the predicted values is often taken as an indication of significant delocalization. For **1**, even if the strong NIR absorption is treated as a single convoluted band, the resulting $\Delta\tilde{\nu}_{1/2}^{exp}/\Delta\tilde{\nu}_{1/2}^{calcd}$ ratio is approximately 0.6 for IT(3,2). A similar relationship was observed for the analogous IT band of **3** measured at 240 K, with $\tilde{\nu} \approx 5.7 \times 10^3$ cm^{-1}, $\varepsilon = 5.0 \times 10^3$ M^{-1} cm^{-1}, $\Delta\tilde{\nu}_{1/2} \approx 2.0 \times 10^3$ cm^{-1}, and a shoulder at higher energy ($\approx 7.5 \times 10^3$ cm^{-1}).[8] No additional low-energy features in the IR region (below 4000 cm^{-1}) were reported for **3**. The mixed-valent form of dimer **2**, in turn, was reported to be unstable toward dissociation and spectroscopic data are not available for comparison.[4]

(21) Demadis, K. D.; Hartshorn, C. M.; Meyer, T. J. *Chem. Rev.* **2001**, *101*, 2655.
(22) (a) Brunschwig, B. S.; Creutz, C.; Sutin, N. *Chem. Soc. Rev.* **2002**, *31*, 168. (b) D'Alessandro, D. M.; Keene, F. R. *Chem. Soc. Rev.* **2006**, *35*, 424. (c) Kaim, W.; Sarkar, B. *Coord. Chem. Rev.* **2007**, *251*, 584.
(23) (a) This classification of mixed-valence systems originates from the classical scheme introduced by Robin and Day. (b) Robin, M. B.; Day, P. *Adv. Inorg. Chem. Radiochem.* **1967**, *10*, 247.
(24) Concepcion, J. J.; Dattelbaum, D. M.; Meyer, T. J.; Rocha, R. C. *Phil. Trans. R. Soc., A* **2008**, *366*, 163.
(25) Rocha, R. C.; Rein, F. N.; Jude, H.; Shreve, A. P.; Concepcion, J. J.; Meyer, T. J. *Angew. Chem., Int. Ed.* **2008**, *47*, 503.
(26) Estimated from spectral deconvolution and curve-fitting analysis assuming a Gaussian lineshape.
(27) Hush, N. S. *Prog. Inorg. Chem.* **1967**, *8*, 391.
(28) Reimers, J. R.; Hush, N. S. *Inorg. Chem.* **1986**, *29*, 3686.

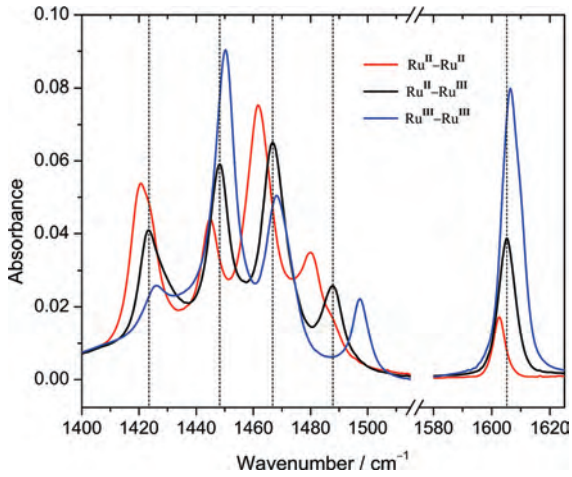

Figure 7. IR spectra of **1** in acetonitrile-d_3. The $Ru^{II}-Ru^{III}$ and $Ru^{III}-Ru^{III}$ species were electrogenerated in situ by stepwise oxidation of the starting $Ru^{II}-Ru^{II}$ complex at 0.4 and 1.0 V vs Ag/Ag^+, respectively. The oxidation steps were fully reversible and the initial spectrum of $Ru^{II}-Ru^{II}$ was recovered upon reduction.

Table 3. Summary of Frequencies (cm^{-1}) for Selected bpy Vibrations in **1**a

	mode 1	mode 2	mode 3	mode 4	mode 5
$Ru^{II}-Ru^{II}$	1420	1445	1462	1480	1602
$Ru^{II}-Ru^{III}$	1423	1448	1466	1488	1605
$Ru^{III}-Ru^{III}$	1426	1450	1468	1497	1607

[a] Pyridyl ring stretching and deformation modes; see ref 30 for detailed assignment based on normal-coordinate analysis.

Together with the estimated $\Delta\tilde{\nu}_{1/2}^{exp}/\Delta\tilde{\nu}_{1/2}^{calcd}$ ratio of ~0.62 for the lowest-energy IT(1) band, these qualitative considerations suggest strong coupling and extensive delocalization in **1**. This precludes the estimation of the magnitude of electronic coupling (H_{ab}) from spectral analysis of IT bands by application of the Mulliken−Hush formalism,[27] which is appropriate for fully localized (class II) systems.[23] Also important to support the above interpretations is the observation that the IT absorptions are independent of solvent in deuterated dichloroethane, acetonitrile, and dimethylformamide.[29] Consistent with the very large value of K_c derived from the electrochemical data, these findings seem to indicate that **1** is strongly coupled, with a delocalized or nearly delocalized mixed-valent state. As recently pointed out, however, conclusions based solely on IT band widths and solvatochromism are not sufficient to delineate localization vs delocalization.[24] The fact that IC bands were not found for $Ru^{II}-Ru^{III}$ could also be taken as supporting evidence for averaging of oxidation states,[21] but the extremely low absorptivity of these low-energy IR bands in the case of Ru complexes impairs the use of this criterion without ambiguity. In such cases, more direct probes are provided by vibrational observables.[21,24]

Vibrational Spectra. The IR spectra in the region from 1400 to 1650 cm^{-1} (Figure 7 and Table 3) exhibit a characteristic set of five vibrational peaks that are assigned to the pyridyl ring stretching and deformation modes of the bpy ligands.[30] Consistent with previous observation for Os(II)/Os(III) systems,[31,32] the frequencies of these bpy modes are systematically upshifted by at least 5 cm^{-1} upon oxidation of $Ru^{II}-Ru^{II}$ into $Ru^{III}-Ru^{III}$. Because they originate at the terminal ligands, such "spectator" vibrations have been used as markers for the oxidation state associated with each of the metal centers in the corresponding mixed-valent complexes.[21,24] From analysis of the spectral lineshapes and comparison of the peak frequencies collected in Table 3 for **1** at all three oxidation states (as determined by IR spectroelectrochemistry), it is clear that the bpy vibrations in $Ru^{II}-Ru^{III}$ result in single peaks with frequencies intermediate between those of $Ru^{II}-Ru^{II}$ and $Ru^{III}-Ru^{III}$. These features are therefore consistent with line coalescence rather than a spectral sum of the oxidized (Ru^{III}) and reduced (Ru^{II}) moieties in the "mixed-valent" state. This type of phenomenon is typical of strongly coupled systems at the delocalized (class III) or localized-to-delocalized (class II−III) regimes[21,24] and has been utilized to probe fast electron-transfer dynamics within the vibrational time domain.[33,34] IR line broadening and coalescence occur if there is site exchange (due to chemical or electronic processes) during the excited-state lifetime of the corresponding vibrations and, therefore, depend on the exchange rate constant and the difference/shift in vibrational frequency ($\Delta\tilde{\nu}$) between the exchanging sites (i.e., Ru^{II} and Ru^{III}). In the case of the bpy vibrations in **1**, where 5 $cm^{-1} < \Delta\tilde{\nu} < 17$ cm^{-1} for the frequencies noted above, the total coalescence observed in Figure 7 provides direct evidence for rapid exchange and valence averaging on the 1−10 ps time scale.[21,34]

Another probe for characterizing valence localization vs delocalization is the presence/absence of IR activity in totally symmetric vibrations at the bridging ligand.[21,24] This tool has been applied to the study of mixed-valence systems bridged by pyrazine, for which the ν_{8a} mode around 1600 cm^{-1} serves as a marker for symmetry breaking/averaging.[31,35] Although three totally symmetric (A_1) vibrations corresponding to in-plane ring deformation modes are known for pyrazolate (C_{2v}) in the 1100−1500 cm^{-1} region,[36,37] IR absorptions from the related bridging vibrations in **1** are either absent or too weak (compared to those of bpy) to be unequivocally characterized. Again, this observation seems to confirm that the dynamics of electron exchange in **1**, at the "mixed-valent" ground state, is fast enough that the oxidation states appear to be averaged even on the time scale of the vibrational periods intrinsic to these modes (ca. 20−30 fs).

(29) (a) These solvents were selected to cover a wide range in the Donor Number scale of solvents. (b) Marcus, Y. *Chem. Soc. Rev.* **1993**, *22*, 409.
(30) Mallick, P. K.; Danzer, G. D.; Strommen, D. P.; Kincaid, J. R. *J. Phys. Chem.* **1988**, *92*, 5628.
(31) Demadis, K. D.; Neyhart, G. A.; Kober, E. M.; White, P. S.; Meyer, T. J. *Inorg. Chem.* **1999**, *38*, 5948.
(32) Rocha, R. C.; Shreve, A. P. *Inorg. Chem.* **2004**, *43*, 2231.
(33) (a) Ito, T.; Hamaguchi, T.; Nagino, H.; Yamaguchi, T.; Washington, J.; Kubiak, C. P. *Science* **1997**, *277*, 660. (b) Londergan, C. H.; Kubiak, C. P. *Chem.—Eur. J.* **2003**, *9*, 5963.
(34) Grevels, F.-W.; Kerpen, K.; Klotzbucher, W. E.; McClung, R. E. D.; Russell, G.; Viotte, M.; Schaffner, K. *J. Am. Chem. Soc.* **1998**, *120*, 10423.
(35) Rocha, R. C.; Shreve, A. P. *Chem. Phys.* **2006**, *326*, 24.
(36) (a) Vos, J. G.; Groeneveld, W. L. *Inorg. Chim. Acta* **1978**, *27*, 173. (b) Cardini, G.; Muniz-Miranda, M. *J. Phys. Chem. B* **2002**, *106*, 6875.

Conclusions

The structural and electronic characterization of a mixed μ-pyrazolate-,μ-alkoxide-bridged dimer of Ru-polypyridine is presented here. Despite its "hybrid" structure, this pyz/OMe heterobridged complex (**1**) exhibits electronic/redox properties that are not a mere averaging of those observed for the pyz/pyz (**2**) and OMe/OMe (**3**) homobridged analogues.[4,8] In fact, the electrochemical window ($\Delta E_{1/2}$) of the mixed-valent $Ru^{II}-Ru^{III}$ trication is especially wide for **1**, and comparison of the related comproportionation constants across the series (with $K_c(\mathbf{1}) > K_c(\mathbf{3}) \gg K_c(\mathbf{2})$) indicated that the strength of metal−bridge−metal interactions and electronic communication is greater in **1** than both **2** and **3**. This finding is especially remarkable if the larger Ru···Ru separation in **1** compared to **3** is taken into account. Despite the possibility of some weak contribution from direct overlap between Ru d orbitals, strong Ru−Ru bonds require a distance of typically less than 2.4 Å[38] and, therefore, the Ru···Ru separation of 3.7 Å precludes significant contribution from direct Ru−Ru interaction in **1**. Detailed analytical comparisons of the spectroscopic features of **1** at its $Ru^{II}-Ru^{II}$, $Ru^{II}-Ru^{III}$, and $Ru^{III}-Ru^{III}$ redox states using spectroelectrochemistry confirmed the electrochemical results and uniformly suggested that the formally "mixed-valent" complex is very strongly coupled, exhibiting electronic and vibrational signatures that are consistent with either class III or class II−III but approaching true electronic delocalization (i.e., at the transition from class II−III to class III).[21,24]

Acknowledgment. This work was supported by the U.S. Department of Energy through the Laboratory Directed Research & Development (LDRD) program at LANL. The technical assistance of Dr. R. Michalczyk (NMR) and Dr. S. Iyer (mass spectrometry) is gratefully acknowledged.

Supporting Information Available: X-ray crystallographic data. This material is available free of charge via the Internet at http://pubs.acs.org.

IC800719U

(37) (a) The corresponding vibrational frequencies for such modes in the free pyrazolate ligand are predicted at 1127, 1215, and 1471 cm^{-1} (unscaled values) by DFT calculations at the B3LYP/6-311++G** level. (b) Frisch, M. J.; Trucks, G. W.; Schlegel, H. B.; Scuseria, G. E.; Robb, M. A.; Cheeseman, J. R.; Montgomery, J. A., Jr.; Vreven, T.; Kudin, K. N.; Burant, J. C.; Millam, J. M.; Iyengar, S. S.; Tomasi, J.; Barone, V.; Mennucci, B.; Cossi, M.; Scalmani, G.; Rega, N.; Petersson, G. A.; Nakatsuji, H.; Hada, M.; Ehara, M.; Toyota, K.; Fukuda, R.; Hasegawa, J.; Ishida, M.; Nakajima, T.; Honda, Y.; Kitao, O.; Nakai, H.; Klene, M.; Li, X.; Knox, J. E.; Hratchian, H. P.; Cross, J. B.; Bakken, V.; Adamo, C.; Jaramillo, J.; Gomperts, R.; Stratmann, R. E.; Yazyev, O.; Austin, A. J.; Cammi, R.; Pomelli, C.; Ochterski, J. W.; Ayala, P. Y.; Morokuma, K.; Voth, G. A.; Salvador, P.; Dannenberg, J. J.; Zakrzewski, V. G.; Dapprich, S.; Daniels, A. D.; Strain, M. C.; Farkas, O.; Malick, D. K.; Rabuck, A. D.; Raghavachari, K.; Foresman, J. B.; Ortiz, J. V.; Cui, Q.; Baboul, A. G.; Clifford, S.; Cioslowski, J.; Stefanov, B. B.; Liu, G.; Liashenko, A.; Piskorz, P.; Komaromi, I.; Martin, R. L.; Fox, D. J.; Keith, T.; Al-Laham, M. A.; Peng, C. Y.; Nanayakkara, A.; Challacombe, M.; Gill, P. M. W.; Johnson, B.; Chen, W.; Wong, M. W.; Gonzalez, C.; Pople, J. A. *Gaussian 03*, revision D.01; Gaussian, Inc.: Wallingford, CT, 2004.

(38) Cotton, F. A.; Murillo, C. A.; Walton, R. A., Eds. *Multiple Bonds between Metal Atoms*, 3rd ed.; Springer: New York, 2005.